Noncollinear magnetic order in Quasicrystals

E.Y. Vedmedenko,[1] U. Grimm,[2] and R. Wiesendanger[1]
[1] *Institut für Angewandte Physik, Jungiusstr. 11, 20355 Hamburg, Germany*
[2] *Applied Mathematics Department, The Open University, Walton Hall, Milton Keynes MK7 6AA, UK*

Based on Monte-Carlo simulations, the stable magnetization configurations of an antiferromagnet on a quasiperiodic tiling are derived theoretically. The exchange coupling is assumed to decrease exponentially with the distance between magnetic moments. It is demonstrated that the superposition of geometric frustration with the quasiperiodic ordering leads to a three-dimensional noncollinear antiferromagnetic spin structure. The structure can be divided into several ordered interpenetrating magnetic supertilings of different energy and characteristic wave vector. The number and the symmetry of subtilings depend on the quasiperiodic ordering of atoms.

PACS numbers: 71.23.Ft, 75.50.Ee, 75.10.Hk, 75.70.Ak

The last few years have shown a boom in investigations of the spin order in antiferromagnetic films [1, 2] motivated by the dramatic changes in the magnetic properties of such systems induced by frustration. In contrast to the rather well studied spin structure of antiferromagnets on periodic lattices, the antiferromagnetic ordering of quasicrystals is subject of ongoing scientific debate. Whereas an experimental finding of long-range antiferromagnetic order in rare-earth icosahedral quasicrystals [3] turned out to be an artefact [4], theoretical models that deal with magnetism on quasicrystals [5] are known to exhibit long-range magnetic order. Recent inelastic neutron scattering experiments on the Zn-Mg-Ho icosahedral quasicrystal [6] revealed a very peculiar diffuse scattering pattern with icosahedral symmetry at temperatures below 6K. Such a pattern, in principle, can originate from a noncollinear spin arrangement first suggested by Lifshitz from pure geometrical considerations [7–9]. However, real-space magnetic configurations leading to those long wave vector correlations remain obscure despite recent interesting results for quantum spins [5]. Thus, the knowledge about the spin structure on quasiperiodic tilings is of basic importance for experiments as well as for theoretical predictions of new phenomena, which can be expected due to nontrivial frustration effects [15].

The patterns found in our theoretical study provide an explanation for the origin of the antiferromagnetic modulations observed experimentally in Ref. [6]. While the spin order in antiferromagnets is usually characterized by a periodic modulation described by wave vectors on the order of inverse atomic distances, the spin order in antiferromagnetic quasicrystals admits three-dimensional noncollinear structures consisting of several interpenetrating subtilings with longer wave vectors. Here we report on the details of the low-temperature antiferromagnetic ordering and the map of the local frustration for the octagonal tiling.

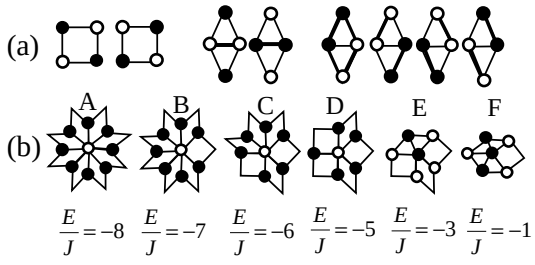

FIG. 1: Configurations for a frustrated Ising antiferromagnet on (a) elementary tiles and (b) six local environments of the Ammann-Beenker tiling. Bold lines denote the frustrated bonds. The open and filled circles represent different spins.

We discuss the antiferromagnetic Hamiltonian

$$H = J_{ij} \sum_{\langle i,j \rangle} \mathbf{S}_i \cdot \mathbf{S}_j - K_1 \sum_i (\mathbf{S}_i^z)^2 \qquad (1)$$

where $\mathbf{S}_i$ is a three- or two-dimensional unit vector in the case of classical vector or xy-spins, and $\mathbf{S}_i^z$ is equal to ± 1 in the case of Ising spins (so $\mathbf{S}_i^x = \mathbf{S}_i^y = 0$); $\langle i,j \rangle$ denotes the nearest neighbor pairs. For an antiferromagnetic system, the exchange parameter J_{ij} is positive, and neighboring antiparallel spins contribute a lower energy than parallel neighbors. The coefficient K_1 is the first-order anisotropy constant. Our Monte-Carlo simulations have been carried out on finite Ammann-Beenker tilings with free boundary conditions. The procedure is a simulated annealing method with at least 15 successive temperature steps [10]. At each temperature, the convergence of the relaxation process towards equilibrium has been observed for any initial configuration after a few thousand Monte Carlo steps per spin. Hence, the single-spin-update algorithm is efficient in our case. At the end of the cooling down process, the total energy is just fluctuating around its mean equilibrium value. To reduce boundary effects only the core of a tiling has been analyzed. The samples

on the octagonal Ammann-Beenker structure, which we shall concentrate on in what follows, are circular, containing 2193, 11664 and 53018 magnetic moments.

The octagonal tiling consists of two motifs: a square and a rhombus of equal edge lengths a (Fig. 1(a)). The diagonal bonds are, usually, neglected in the calculations [5, 11]. We find this disregard physically questionable as the exchange coupling increases exponentially with decreasing interatomic distance. In the present investigation, the short diagonal of the rhombus and the sides of the motifs have been considered as nearest neighbors. We distinguish the two cases $J_d > 2J$ and $J_d < 2J$, where J_d denotes the interaction along the short diagonal and the interaction strength along the sides J is unity. The first case corresponds to a rapid growth of the exchange coupling with decreasing interatomic distance. The two nearest-neighbor bonds form six local environments with coordination numbers varying from 5 to 8 as shown in Fig. 1(b). They occur with relative frequencies $\nu_A = 17 - 12\sqrt{2} \approx 2.9\%$, $\nu_B = -41 + 29\sqrt{2} \approx 1.2\%$, $\nu_C = 34 - 24\sqrt{2} \approx 5.9\%$, $\nu_D = -14 + 10\sqrt{2} \approx 14.2\%$, $\nu_E = 6 - 4\sqrt{2} \approx 34.3\%$, and $\nu_F = -1 + \sqrt{2} \approx 41.4\%$ [12]. Taking into account the short diagonals of the rhombic tiles increases the average coordination number of the tiling from 4 (the value without diagonals) to $8\nu_A + 7\nu_B + 6\nu_C + 5(\nu_D + \nu_E + \nu_F) = 8 - 2\sqrt{2} \approx 5.17$.

First we discuss the Ising system. The square tile of the octagonal structure is non-frustrated as every pair of the moments can be chosen to be antiparallel (Fig. 1(a)). If we had not taken the short diagonals of the rhombic tiles into account, the same would have been true for the entire tiling, and there would be no frustration, because the rhombic tiling is bipartite. Now, we consider spins on short diagonals as nearest neighbors, the rhombic tiles are always frustrated. If the energy of one nearest neighbor pair is minimized by having antiparallel spins, the third and forth spins cannot be chosen to minimize the energy of both of its neighbors (Fig. 1(a)). The magnetic moment will necessarily be parallel to one of the neighbors. For $J_d < 2J$ two out of six possible configurations have smaller energy as they possess only one pair of parallel nearest neighbors per rhombus instead of two (Fig. 1(a)). In this case spins can have one of six possible energy values corresponding to different local environments (Fig. 1(b)). For $J_d > 2J$ the four configurations with two parallel bonds have lowest energy as their weight is smaller than that of the strong diagonal coupling. The second case comprises much more different possibilities of energy distribution. To give a quantitative description of the local frustration we introduce a local parameter f

$$f = \frac{|E_{id}| - |E_i|}{|E_{id}|} \tag{2}$$

where E_i is an actual energy of a spin i and E_{id} is a ground state energy of a relevant unfrustrated vertex. With this nomenclature, only the central spins of the vertices F and E are magnetically frustrated $f_F = 0.4$ and $f_E = 0.8$ for $J_d = J < 2J$. The Monte-Carlo simulations confirm our reasoning based on the analysis of frustration. Fig. 2a gives the frequency distribution of the exchange energy per atom E for two cases and a top-view of a portion of Ising configuration with $J_d > 2J$. The energy distribution for $J_d < 2J$ simply reproduces the frequency of 6 vertex configurations. The "up" and "down" configurations are perfectly ordered and coincide with the black-and-white model of Niizeki [13]. For large J_d we find 8 possible energy values. The "up" and "down" subtilings, however, are spatially disordered (see inset Fig. 2a). We have calculated the magnetic structure factor

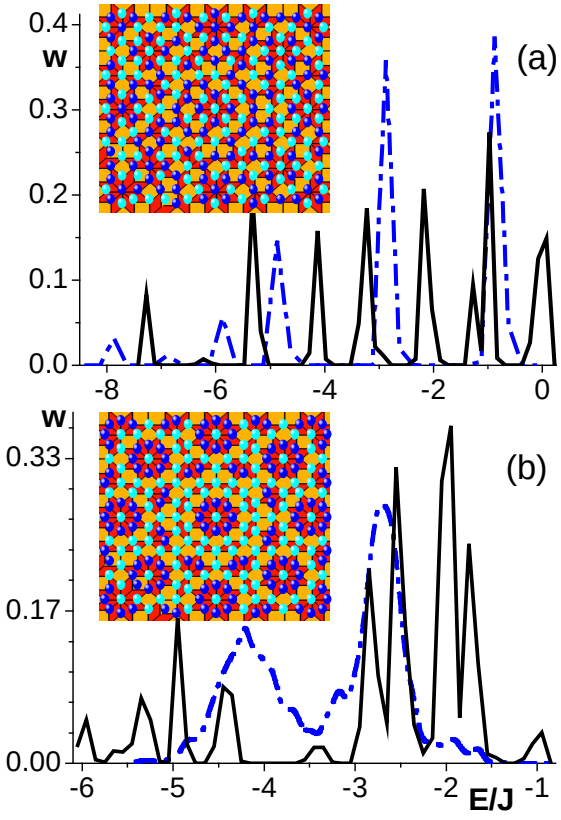

FIG. 2: The frequency distribution of the energy per spin on the octagonal tiling for (a) Ising and (b) vector spins. Solid lines correspond to the case $J_d < 2J$, dashed lines to $J_d > 2J$. Purely antiferromagnetic interaction at $kT = 0.01J$ is considered. Top-views of portions of Monte-Carlo configurations with underlying tilings are shown as insets. The light and dark circles represent different spins in (a) and different energies in (b), respectively.

$$S^{zz}(\mathbf{k}) = \frac{1}{N} \sum_{\mathbf{r},\mathbf{r}'} e^{i\mathbf{k}\cdot(\mathbf{r}-\mathbf{r}')} \langle S^z_{\mathbf{r}} S^z_{\mathbf{r}'} \rangle \tag{3}$$

using the Monte-Carlo data for different samples. Here $\mathbf{k}$ is the wave vector and $S^z_{\mathbf{r}}$ is a vertical component of a magnetic moment at the position $\mathbf{r}$. The diffraction pattern of the Niizeki configuration coincides with that of quantum Monte-Carlo calculations (Fig. 5c,d of Ref. [5])

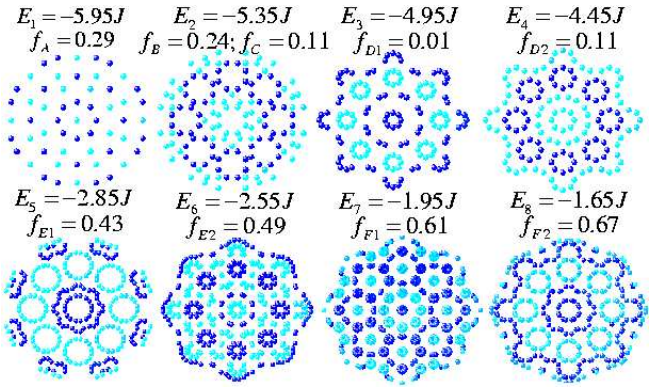

FIG. 3: (color on-line) Spatial distribution of magnetic moments belonging to eight subtilings of a noncollinear configuration on an octagonal tiling consisting of 2193 spins. $J_d > 2J$. The light and dark circles represent positive and negative x-components of the magnetization. The in-plane components are not given for the sake of simplicity. Average values of the exchange energy E and the local frustration f per spin are indicated.

and theoretical prediction [9], while the intensity map of the configuration Fig. 2a is almost structureless. It means that Ising solution with $J_d < 2J$ reproduces in essence the antiferromagnetic superstructure, corresponding to a modulation vector $\mathbf{q} = (\frac{1}{2}, \frac{1}{2}, \frac{1}{2}, \frac{1}{2})_{a^*}$ [6] in the octagonal tiling, whereas stronger coupling leads to a spin-glass state.

An exciting question is if the further minimization of the total energy and frustration by means of the noncollinear alignment of magnetic moments is possible. At first glance the magnetic structure of the low-temperature pure antiferromagnetic configuration seems to be rather disordered. The analysis of the local energies, however, reveals several characteristic energetic maxima in the frequency distribution shown in Fig. 2(b). The simple existence of the peaks means that there exist different sorts of magnetic moments having well-defined relative orientation to their nearest neighbors. This orientation, however, is not associated with any absolute direction in space. Therefore, in accordance with the Mermin-Wagner theorem [14], no long-range order exists in two-dimensions with continuous symmetry, because thermal fluctuations result in a mean-square deviation of the spins from their equilibrium positions which increases logarithmically with the size of the system. The addition of a very weak anisotropy, which often exists in real samples, does not change the distribution of the exchange energy, but permits to anchor the absolute spatial orientation of the magnetization. Nevertheless, at first glance the total structure still looks spin-glass like. In the following, we will show that the antiferromagnetic structure of the octagonal tiling is perfectly ordered, but the order is non-trivial and unusual for periodic crystals. We concentrate further description on 3D vector spins while similar results for xy-spins have been obtained.

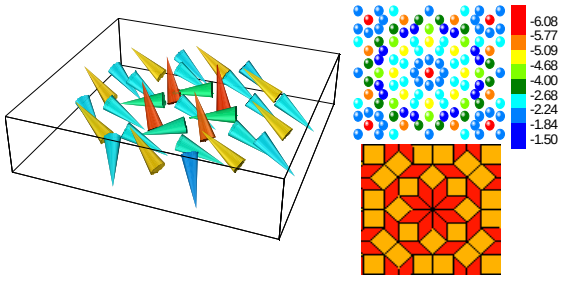

FIG. 4: Perspective view of a portion of a Monte-Carlo configuration on an octagonal tiling. The top view of the patch and the energy map are shown as insets. Magnetic moments are represented as cones. The cones are colored according to their vertical magnetization, changing gradually from red for "up" to blue for "down" spins. In the energy map inset, the colors encode the energy per moment.

To obtain an absolute symmetry axis, we apply a very weak out-of-plane anisotropy $K_1 \approx 10^{-3}J$ to the system. The squared vertical component of magnetization $(S^z)^2$ becomes finite. The positions of the energy peaks on the frequency diagram remain unchanged. All maxima are different from those of the Ising model. It means that the angles between the neighboring magnetic moments are not always equal to 180° or 0°, i.e., the magnetic structure is noncollinear. The different number of peaks — eight for $J_d < 2J$ and two for $J_d > 2J$ (Fig. 2(b)) — already tells us that, in contrast to the Ising case, the maxima do not coincide with the 6 vertices of the tiling. The minimal possible local energy increases from $-8J$ to approximately $-6J$ for $J_d = J$ or $-5.44J$ for $J_d = 2.2J$. The average energy per spin, however, decreases by more than $0.3J$ and reaches the value of $E \approx -2.85J$ and $E \approx -3.30J$ respectively. Hence, the increase of the entropy permits to minimize the average frustration and the total energy of the system.

Spatial arrangements of the magnetic moments as a function of the exchange energy are given in Fig. 3 for $J_d < 2J$ and in the inset to Fig. 2(b) for $J_d > 2J$. Each configuration of Fig. 3 represents a certain energy range corresponding to one of the eight peaks in the spectrum of Fig. 2(b). Colors represent the x-projection of the magnetization. The magnetic moments form 8 subtilings of different energy $(E_1, \ldots, E_8)$ which generally do not coincide with a specific vertex type. The splitting of the energy and frustration levels is described in detail in Fig. 3. For example the vertices B and C (Fig. 1 belong to the same energy maxima E_2 but have different local frustration $f_B = 0.24$, $f_C = 0.11$ (Fig. 3). At the same time the central spin of the vertex D can have either the energy E_3 or E_4 and, therefore, can have two different values of the frustration $f_{D1} = 0.01$ and $f_{D2} = 0.11$ depending on local surroundings. Thus, every configuration of the Fig. 3 can enclose either a part of the atomic places belonging to one vertex type or two different vertex types together. Nevertheless all structures have a perfect general spatial ordering. Each subtiling

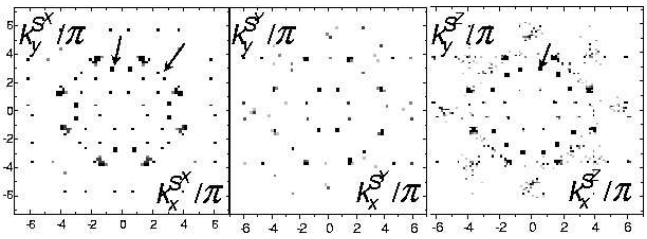

FIG. 5: The calculated Bragg scattering of S^x, S^y and S^z component of magnetization for the antiferromagnetic superstructure. Reflexes indicated by arrows are new in comparison to previous studies [5].

can be separated into the energetically degenerate 'right' and 'left' parts which also have a perfect quasiperiodic arrangement. However, not all 'right' or 'left' moments have identical orientation in space. Fig. 4 shows a perspective view of a portion of typical Monte-Carlo configuration and corresponding energy map. The central magnetic moment has the lowest energy and belongs to the E_1 subtiling. Its 8 nearest neighbors have identical energies and correspond to the energy E_7 despite having different sets of mutual angles. The moments forming the next ring have energy E_6. The last ring consists of the alternating E_3 and E_6 spins. Fig. 4 shows one of the radially symmetric vertices. However, in the octagonal tiling vertices with different surrounding can also be found. The energy distribution is then different. Hence, the magnetic structure for $J_d < 2J$ is noncollinear and consists of eight interpenetrating subtilings. For $J_d > 2J$ we find only two subtilings of different energy.

A frequency distribution of the angle between nearest neighboring moments shows five characteristic angles close to 60°, 80°, 120°, 140° and 180° for small J_d and a single mutual angle of 110° for large J_d. Due to this noncollinearity the energy of the system is decreased. The diffraction pattern of the whole structure is more complex than that of the Ising or the quantum-mechanical [5] model. As the spin structure is noncollinear, not only the structure factor S^{zz}, but also S^{xx} and S^{yy} can be recognized (see Fig. 5). The eightfold S^{xx} and S^{zz} patterns contain additional long wave-vector peaks which could not be identified in the previous investigations [5]. In dependence on the anisotropy (or on the initial random configuration for $K_1 = 0$) new peaks also occur in S^{yy}. The Bragg reflexes found in our study select a subset of the wave vectors given in Ref. [9] where $n_1+n_2+n_3+n_4$ is odd. Peaks with $n_1 + n_2 + n_3 + n_4$ even are extinct. According to the nomenclature of Ref. [9], the following wave vectors can be identified: $(1, 0, 0, 0)$, $(1, -1, 1, 0)$, $(3, -2, 1, 1)$, $(3, -1, -1, 2)$, $(1, 1, -1, 0)$, $(1, 0, 1, -1)$, $(0, 2, -1, 0)$, $(0, 0, 1, -2)$, $(-1, 0, 1, -3)$, $(0, 2, -2, 1)$, $(0, 1, -2, 2)$. Hence, the noncollinearity of the spin structure gives rise to selection rules different from those of collinear models [5, 7]. With increasing sample size the peaks become more diffuse and may correspond to the diffuse scattering signal of Ref. [6].

In conclusion, we demonstrate that the frustrated classical Ising system with antiferromagnetic coupling on a quasiperiodic octagonal tiling is perfectly ordered. All spins can be divided into 6 quasiperiodic (in the 3D physical space) or 6 periodic (in 6D periodic crystal) subtilings of different energy. Each subtiling corresponds to the one of 6 vertex types of the Ammann-Beenker structure and is degenerated for 'up' and 'down' magnetic moments. Quantitatively, only two out of six subtilings are frustrated with the local coefficients $f_E = 0.4$ and $f_F = 0.8$. The vector spin system admits a three-dimensional noncollinear magnetic structure. For $J_d < 2J$, the whole structure can be decomposed into 8 subtilings of different energy which generally do not coincide with a specific vertex type. All subtilings are frustrated. However, the total degree of frustration and the energy of the system is minimized compared to the noncollinear case. The subtilings are degenerated with respect to the spin direction. The codirectional spins of every subtiling reveal perfect quasiperiodic ordering with a wave vector which is specific for a given subtiling.

We thank R. Lifshitz for helpful comments and indexing of the Bragg peaks. Financial support from the Interdisciplinary Nanoscience Center Hamburg (INCH) is gratefully acknowledged.

REFERENCES

[1] Ph. Kurz, B.H. Bihlmayer, K. Hirai, and S. Blügel, Phys. Rev. Lett. **86**, 1106 (2001).
[2] S. Heinze, M. Rode, A. Kubetzka, O. Pietzsch, X. Nie, S. Blugel, R. Wiesendanger, Science **288**, 1805, (2000).
[3] B. Charrier, B. Ouladdiaf, and D. Schmitt, Phys. Rev. Lett. **78**, 4637 (1997).
[4] T. J. Sato, H. Takakura, A. P. Tsai, and K. Shibata, Phys. Rev. Lett. **81**, 2364 (1998).
[5] S. Wessel, A. Jagannathan, and S. Haas, Phys. Rev. Lett. **90**, 177205 (2003).
[6] T.J. Sato, H. Takakura, A.P. Tsai, K. Shibata, K. Ohoyama, and K.H. Andersen, Phys. Rev. B **61**, 476 (2000).
[7] R. Lifshitz, Mater. Sci. Eng. A **294**, 508 (2000).
[8] R. Lifshitz, Phys. Rev. Lett. **80**, 2717 (1998).
[9] R. Lifshitz, Acta Cryst. A **60**, 167 (2004).
[10] E.Y. Vedmedenko, H.P. Oepen, and J.Kirschner, Phys. Rev. Lett. **90**, 137203 (2003).
[11] U. Grimm and M. Baake, Aperiodic Ising Models, in *The Mathematics of Long-Range Aperiodic Order*, edited by R.V. Moody (Kluwer, Dordrecht, 1997) pp. 199.
[12] M. Baake and D. Joseph, Phys. Rev. B **42**, 8091 (1990).
[13] K. Niizeki, J. Phys. A: Math. Gen.**23**, 5011 (1990).
[14] N.D. Mermin and H. Wagner, Phys. Rev. Lett. **17**, 1133 (1966).

[15] G.G. Naumis, R. A. Barrio, and C. Wang, Phys. Rev. B **50**, 9834 (1994).